Single Molecule Mechanical Probing of the SNARE Protein Interactions

W. Liu,*§ Vedrana Montana,†‡§ Jihong Bai,¶ Edwin R. Chapman,¶ U. Mohideen,*§ and Vladimir Parpura†‡§

*Departments of Physics and †Cell Biology & Neuroscience, ‡Centers for Glial-Neuronal Interactions, and §Nanoscale Science & Engineering, University of California, Riverside, California 92521; and ¶Department of Physiology, University of Wisconsin, Madison, Wisconsin 53706

ABSTRACT   Exocytotic release of neurotransmitters is mediated by the ternary soluble N-ethyl maleimide-sensitive fusion protein attachment protein receptors (SNAREs) complex, comprised of syntaxin (Sx), synaptosome-associated protein of 25 kDa (SNAP25), and synaptobrevin 2 (Sb2). Since exocytosis involves the nonequilibrium process of association and dissociation of bonds between molecules of the SNARE complex, dynamic measurements at the single molecule level are necessary for a detailed understanding of these interactions. To address this issue, we used the atomic force microscope in force spectroscopy mode to show from single molecule investigations of the SNARE complex, that Sx1A and Sb2 are zippered throughout their entire SNARE domains without the involvement of SNAP25. When SNAP25B is present in the complex, it creates a local interaction at the 0 (ionic) layer by cuffing Sx1A and Sb2. Force loading rate studies indicate that the ternary complex interaction is more stable than the Sx1A-Sb2 interaction.

INTRODUCTION

Exocytosis underlies the release of transmitters from neurons and astrocytes (1,2) in the central nervous system. After increase of the intracellular Ca^{2+} level, transmitter molecules stored in secretory vesicles are released into the extracellular space. This secretory process at presynaptic terminals is mediated by the core complex containing the soluble N-ethyl maleimide-sensitive fusion protein attachment protein receptors (SNAREs), including synaptobrevin 2 (Sb2; also referred to as vesicle-associated membrane protein 2, VAMP2), synaptosome-associated protein of 25 kDa (SNAP25), and syntaxin (Sx) (3,4). Over the last few years structural, biochemical, biophysical, and genetic studies have provided critical insights into the assembly of this complex, yet the exact nature of the role of the individual SNARE proteins in the complex is debated.

Until recently, a view of the SNARE complex formation assumed a Sx1-SNAP25 intermediate binary complex located at the plasma membrane, which forms the core (ternary) SNARE complex, necessary for vesicular fusion, when it interacts with Sb2 located on vesicles. However, experiments using either Clostridial toxins that cleave Sb, or genetically engineered organisms (*Saccharomyces cerevisiae*, *Caenorhabditis elegans*, *Drosophila*, and mouse) lacking the vesicular-SNARE Sb showed that the vesicular fusion was not completely abolished (5–11). For example, electrophysiological examination in *Drosophila* lacking neuronal Sb showed that even though action potential-evoked synaptic transmission was abolished, spontaneous vesicular fusions were still recorded although at a reduced rate; ultrastructurally, vesicles were targeted to the presynaptic terminals and they docked normally (9). Similarly, in squid giant presynaptic terminals injected with botulinum toxin C1, which cleaves Sx, vesicles were docked normally, whereas evoked synaptic transmission was abolished (12). Furthermore, in *Drosophila* strains lacking Sx both evoked and spontaneous synaptic transmission were abolished, whereas docking was preserved (9). Therefore, it seems that both proteins Sb and Sx have a postdocking function in vivo, with Sb having a prefusion role, whereas Sx could have a central role in vesicular fusion. Indeed, transmembrane segments of Sx line the fusion pore of regulated exocytosis (13,14). Genetic ablation of the plasma membrane target-SNARE SNAP25 in mouse revealed that spontaneous, but not evoked synaptic transmission, can occur in the absence of this protein (15). Taken together, the persistence of fusion in these experiments when using live cellular systems perhaps is due to the redundancy of cellular proteins; closely homologous proteins could substitute the eliminated ones and rescue the function. Consistent with this notion, members of Sb family in *Drosophila* are functionally interchangeable for synaptic transmission (16). Thus, it appears that in vivo there could be many interactions between SNARE proteins mediating fusion with some redundancy and promiscuity in these interactions.

To study exocytosis at the molecular level, one can in vitro reconstitute docking and fusion by using purified recombinant proteins and artificial membranes. Here, in the absence of all other proteins otherwise present in vivo the SNAREs mediate both docking and fusion in vitro. For instance, fusion of modified synaptic vesicles or large-dense core neurosecretory granules containing native vesicular-SNARE(s) to a planar lipid bilayer containing Sx1A, but not SNAP25, has been reported (17,18). Additionally, Sx1A in supported bilayers and Sb2 in liposomes are necessary and sufficient to mediate liposome docking and fusion, which occurred even

without SNAP25; the presence of SNAP25 had little effect on docking efficiency and the probability of fusion (19,20). This is in sharp contrast with the results from studies using proteoliposomes fusing to each other when reconstituted with SNARE proteins, where the fusion was inhibited either by botulinum toxins A and E, which cleave SNAP25, or by an antibody against SNAP25 (21,22). Therefore, it would be important to further comparatively investigate the roles of Sx-Sb and SNAP25-Sx-Sb complexes in docking and fusion in vitro; these investigations should increase our understanding of intermolecular interactions between the protein components of these complexes.

Fusion of single synaptic vesicles to the neuronal plasma membrane has been investigated using electron microscopy (23), amperometry (24), total internal reflection fluorescence microscopy (25), and capacitance measurements (26) (also reviewed in Ryan and Reuter (27)). In these approaches, vesicular fusion was clearly defined by detecting Ω shapes, amperometric spikes, the loss of recycling dyes, or capacitance step increases, respectively. Even though docking of a single vesicle is experimentally less accessible, this process was studied using electron microcopy, where vesicles in close apposition to the plasma membrane were considered to be docked (9,12,28). A dynamic imaging study of docking in neurons, which assessed the formation of stable SNAP25-Sb2 complexes, was done using fluorescence resonant energy transfer (FRET) and wide-field fluorescence microscopy (29), although not at the level of single synaptic vesicles. Additionally, dynamics of the interactions between SNARE proteins were thoroughly investigated using biochemical and biophysical approaches, including surface plasmon resonance (e.g., Calakos et al. (30)). However, the process of association and dissociation of the bonds between molecules of the SNARE complex is inherently a nonequilibrium process and therefore equilibrium-binding constants that are usually measured in biochemical test-tube approaches might not provide the complete information. Consequently, dynamic measurements at the single molecule level would be necessary for better understanding of intermolecular interactions of proteins within the SNARE complex. A prerequisite for designing such measurements is the existence of precise molecular structure of SNARE proteins, which has recently been accomplished using x-ray crystallography (31). Indeed, cleverly designed single molecule studies, guided by the available x-ray crystallography structural information using FRET and total internal reflection fluorescence microscopy further advanced our understanding of SNARE protein interactions and their role in exocytosis (19,32). However, these studies could not offer information on the mechanical characteristics of the protein interactions, a necessary component for detailed understanding of exocytosis. Relatively recently, the atomic force microscope (AFM) has emerged as a powerful tool for studying single molecule nanomechanical interactions (33–37). Parameters that can be measured using AFM spectroscopy, such as the force and the total mechan-

ical extension (strain) required to rupture the binding between the various proteins, can yield valuable insight into the sequence of interactions, the nature of the binding (zippering versus highly localized binding site), and the strength of the binding. The initial study of SNARE proteins by the AFM spectroscopy used only the rupture force as a representation of the binding energy in understanding single molecule interactions between SNARE proteins (37). However, the work done, which is a vector product of the applied force and the corresponding extension, is accounted in part by the energy for breaking of the intermolecular bonds, in part by the energy required to compensate the thermal entropy of the free sections of the stretched proteins and dissipation. The final force required to rupture all the bonds will not necessarily correspond to the total interaction energy of the bound proteins (as assumed in Yersin et al. (37)) due to: 1) the different extensions for each system; 2) unknown angle of the applied force with respect to the axis of the protein system; 3) entropy contributions; and 4) dissipation.

Here we extend AFM spectroscopy measurements using experimental conditions emulating physiological ones. We show from single molecule mechanical investigations of the SNARE complex that both the total extension and the force provide critical information on the binding mechanism. Hence, in the case of Sx1A and Sb2 interactions, the single molecular pair measurements under different force loading rates confirm a zippering model, i.e., formation of coiled coils (30,38). In contrast, in the ternary SNARE complex where SNAP25B is additionally present, the measured extension (~12 nm) is consistent with the position of the localized electrostatic bond (0 or ionic layer) predicted from x-ray structure (31). Additionally, the Sx1A-Sb2 interaction has an order of magnitude higher dissociation rate than the rate determined for the ternary complex. Thus, the presence of SNAP25B in the complex would allow positioning of vesicles at a maximal distance of ~12 nm from the plasma membrane for an extensive period of time, when compared to the period permitted by the Sx1A-Sb2 interactions alone. These findings support similar conclusions drawn from other techniques.

METHODS

Recombinant proteins

Recombinant Sb2 and Sx1A were generated using modified pET vectors as described elsewhere (39,40), resulting in their cytoplasmic domains (aa 1–94 of rat Sb2 and aa 1–266 of rat Sx1A) tagged with six histidines (H6) at their C-termini (Sb2-H6 and Sx1A-H6). Similarly, we also generated C-terminus H6-tagged truncated form of rat Sx1A (Sx1A$_{178-266}$-H6) containing SNARE domain (aa 178–266), but lacking an N-terminal part of the molecule. Recombinant N-terminally H6-tagged full-length rat SNAP25B (H6-SNAP25B) was generated using pTrcHis vector. These proteins were purified using nickel-sepharose beads (Qiagen, Valencia, CA). Recombinant full-length rat SNAP25B was generated using pGEX-2T vector and expressed as a fusion protein having glutathione S-transferase (GST) at its N-terminus (GST-SNAP25B). We also generated cytoplasmic domains of Sb2 and Sx1A (aa 1–94 and aa 1–265 of rat sequences, respectively) tagged

with GST at their N-termini (GST-Sb2 and GST-Sx1A). The resulting GST fusion proteins and GST alone were purified using glutathione columns (Amersham Biosciences, Piscataway, NJ). The proteins were quantified using the Bradford reagent (Pierce Biotechnology, Rockford, IL) and bovine serum albumin as a standard. To determine their purity, the proteins were subjected to 15% sodium dodecyl sulfate-polyacrylamide gel electrophoresis in combination with silver-stain technique (41). Densitometry of silver-stained gels, performed using ChemiDoc XRS gel documentation system (BioRad Laboratories, Hercules, CA), indicated that purified recombinant proteins represent 84–97% of the total protein content.

Western blotting

Recombinant proteins were loaded at 1 μg per lane and subjected to 15% sodium dodecyl sulfate-polyacrylamide gel electrophoresis, followed by transfer to nitrocellulose membranes that were probed with antibodies against Sb2 (clone 69.1, Synaptic Systems, Goettingen, Germany, catalog No. 104 201, 1:1000 dilution; note that this product has been recently replaced by the manufacturer with catalog No. 104 211), SNAP-25 (clone 71.1, Synaptic Systems, catalog No. 111 001, 1:10,000 dilution), and Sx1 (clone 78.2, Synaptic Systems, catalog No. 110 001, 1:10,000 dilution or clone HPC-1, Sigma-Aldrich, catalog No. S0664, 1:1000 dilution). Immunoreactivity of bands was detected using enhanced chemiluminescence (Amersham Biosciences, Piscataway, NJ). All proteins showed single immunoreactive bands with appropriate molecular weights.

In experiments using light chain of botulinum toxin B (BoNT-B; List Biological Laboratories, Campbell, CA) we incubated 200 ng of toxin with 1 μg of recombinant Sb2 in internal solution containing 250 μM zinc chloride at room temperature (20–24°C) for 2 h whereupon the reaction was stopped by adding 3× gel sample buffer. The internal solution contained (in mM): potassium-gluconate, 140; NaCl, 10, and HEPES, 10 (pH = 7.35). The cleavage of Sb2 was assessed using anti-Sb2 antibody (clone 69.1), which was raised against synthetic peptide corresponding to the N-terminal part of rat Sb2 (aa 1–17, but Met1 was replaced by Cys) (42). Although this epitope is still present in BoNT-B cleavage product (aa 1–76), it is not recognized by this antibody for unknown reasons, as described elsewhere (e.g., Fig. 4 of Parpura et al. (43)). Consequently, Western blots show reduction in the single immunoreactive band without displaying an additional lower molecular weight band. Furthermore, the activity of BoNT-B was confirmed using previously described micromechanosensor (44).

Functionalization of cantilevers and glass coverslips

Triangular silicon nitride cantilevers (320 μm long; Digital Instruments, Santa Barbara, CA) with integral tips and glass coverslips (Fisher Scientific; catalog No. 12-545-82-12CIR-1D) were coated with nickel films (thickness ~150 nm) using a thermal evaporator. After nickel film deposition, the tips were functionalized with Sx1A-H6 recombinant proteins by incubating tips in a solution containing proteins (aa 1–266 and aa 178–266 at 0.1–0.2 mg/mL and 0.5 mg/mL, respectively) for 3 h at room temperature. In some experiments, the tips were functionalized with synthetic H6 peptide (10 mg/mL; Covance Research, Berkeley, CA; catalog No. PEP-156P). Nickel-coated glass coverslips were functionalized with Sb2-H6 recombinant protein or H6 by applying a solution containing protein (0.17 mg/mL) or peptide for 1 h at room temperature. After incubation with recombinant proteins or synthetic H6 peptide, the tips and coverslips were rinsed three times with an internal solution, and then were kept separately submersed in this internal solution in a humidified chamber at +4°C until used in experiments for up to 36 h. Before experiments the glass coverslips were mounted on metal disc AFM sample holders.

In some experiments, a solution containing either GST-Sb2 (2.3 mg/mL), GST-SNAP25B (0.475 mg/mL), or GST alone (2.125 mg/mL) was applied onto Sx1A functionalized tips for 10–30 min at room temperature, followed by a triple wash with internal solution. In a subset of experiments, we further treated Sb2 functionalized coverslips in three different ways: 1) Internal solution supplemented with light chain of BoNT-B (100 nM) and zinc chloride (250 μM) was applied onto functionalized coverslips at room temperature for 2 h (used for indirect immunochemistry; compare this to the BoNT treatment used in single molecule measurements in the next section, Force-distance curves; zinc ions alone do not significantly affect the nickel-histidine coordination (44)). 2) GST-Sx1A (0.7 mg/mL) or GST (2.125 mg/mL) alone was applied onto Sb2 functionalized coverslips for 30 min at room temperature. 3) Peptides encoding for rat Sx1A aa 178–200 and aa 215–235 (Synthetic Biomolecules, San Diego, CA) dissolved in internal solution (1 mg/mL each) were separately applied onto Sb2 functionalized coverslips for 30 min at room temperature. After any of these treatments, coverslips and tips were rinsed three times with internal solution and stored in a humidified chamber at +4°C until used in experiments.

When Sx1A-H6 was combined with Sb2-H6, H6-SNAP25B (0.1 mg/mL), or H6 and used for cofunctionalization, these agents were preincubated in equimolar ratio in a tube for 10 min at room temperature before they were coapplied onto coverslips or tips for 1 and 3 h at room temperature, respectively. Cofunctionalization of tips and coverslips with Sx1A-H6 + Sb2-H6 and tips with Sx1A-H6 + H6-SNAP25B or Sx1A-H6 + H6 was followed by rinsing them three times with internal solution. They were then stored in a humidified chamber at +4°C until used in experiments.

To accommodate for variations in the success of procedures used for functionalization of tips and coverslips, we performed matching controls with any of the treatments to allow for day-to-day comparison of the data.

Force-distance curves

We used nanoscope E and associated equipment (Digital Instruments, Santa Barbara, CA) in force spectroscopy mode. All experiments were carried out at room temperature (20–24°C) in a fluid cell that kept hydration and osmotic properties of the sample. Force was calculated using spring constants, ranging from 10 to 13 mN/m that were determined for each cantilever using a previously described method (45). The bending of the cantilever was taken into account in the calculation of the extension (46). The piezoelectric tube extension, including nonlinearities, was calibrated interferometrically for all force loading rates used (47). All extension and force measurements are expressed as mean ± SE.

In experiments using light chain of BoNT-B, internal solution was supplemented with BoNT-B (100 nM), zinc chloride (250 μM), tetrakis-(2-pyridilmethyl)ethylenediamine (TPEN; 50 μM; Molecular Probes, Eugene, OR; catalog No. T1210) or with some combinations of these agents. This solution was injected into the fluid cell using microfluidic ports, resulting in 5.7-fold dilution of BoNT-B, Zn^{2+}, and TPEN. The final concentrations of these agents reported in this work were adjusted to accommodate dilution factors. In a subset of the experiments, internal solution alone (sham treatment) was injected using the same protocol. The acquisition of force-distance curves in these experiments was executed twice: once just before the treatment and then again 23–31 min after the initiation of the treatment (injection of solution). In the experiments where a combination of BoNT-B and TPEN was used, these agents were preincubated on ice for 1 h, followed by equilibration at room temperature (~25 min) before injection into the fluid cell.

Strength of single molecule binding force between six consecutive histidine molecules (H6) tag and Ni²⁺

H6 functionalized coverslips were incubated with nickel-agarose bead suspension (Qiagen, catalog No. 36111; 20–70 μm in diameter) for 5 min at room temperature. The coverslips decorated with beads were then rinsed with internal solution to remove the excess of nonadherent beads. The remaining attached beads were then probed with H6 functionalized tips. The

mean value of the single molecule binding force between H6 and Ni^{2+} was found to be 525 ± 41 pN (32 events) by measuring the force required to rupture the attachment of H6 functionalized AFM tips to the nickel-agarose bead. These forces were much greater than the forces measured for taking apart recombinant proteins studied. Additionally, the force measurements are in good agreement with previously reported mechanical strength of the coordination bond between an H6 tag and nickel nitrilotriacetate (48).

Indirect immunochemistry

The presence of Sx1A and SNAP25B on functionalized tips and Sb2 on functionalized glass coverslips was determined by indirect immunochemistry. We labeled tips and glass coverslips using mouse monoclonal antibodies against Sx1 (clone HPC-1, 1:500) and against Sb2 (1:500), respectively. In experiments where SNAP25B was complexed onto Sx1A functionalized tips, SNAP25B was probed with a rabbit polyclonal antibody (clone MC-21, 1:200) generously supplied by Dr. Pietro DeCamilli (Yale University, New Haven, CT). Cantilevers were incubated with the primary antibodies for 1 h at room temperature and followed by triple wash with internal solution. The TRITC-conjugated goat anti-mouse or Alexa Fluor 488-conjugated goat anti-rabbit (Molecular Probes) secondary antibodies were applied and the preparation was incubated for 1 h at room temperature followed by a triple washout in internal solution.

Visualization for immunochemistry was done using an inverted microscope (Nikon TE 300) equipped with wide-field epifluorescence (Opti-Quip, Highland Mills, NY; 100 W xenon arc lamp), and standard fluorescein (for Alexa Fluor 488) and rhodamine (for TRITC) filter sets (Chroma Technology, Brattleboro, VT). Images were captured through the $20\times$ air (for cantilevers) and $60\times$ oil immersion (for coverslips) objectives using a CoolSNAP-HQ cooled charge-coupled device camera (Roper Scientific, Tucson, AZ) driven by V++ imaging software (Digital Optics, Auckland, New Zealand). To reduce photobleaching of the sample an electronic shutter (Vincent Associates, Rochester, NY) was inserted in the excitation pathway and controlled by the software. Bright-field images were acquired with a green interference filter inserted in the light path of a halogen lamp. All images presented in the figures represent raw data.

RESULTS

We measured the interaction between single molecule pairs of Sb2 and Sx1A using single molecule force spectroscopy
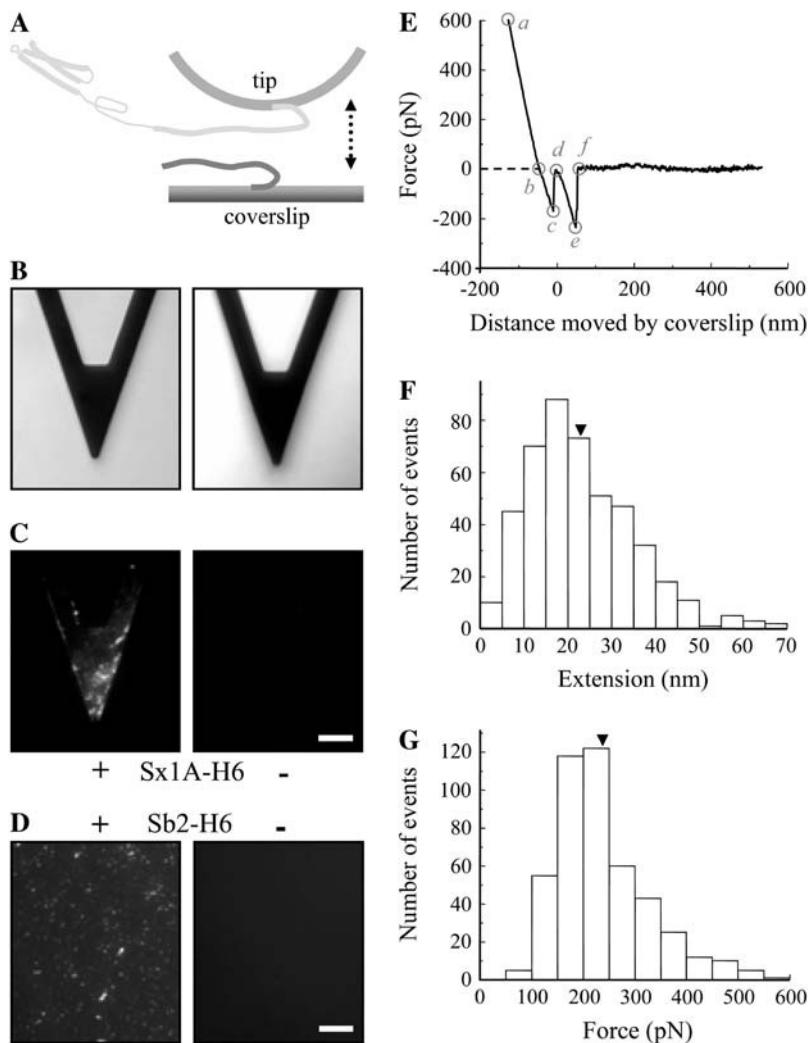

FIGURE 1 (*A*) Schematic of experimental approach. Recombinant Sb2 (Sb2-H6) is attached to the nickel-coated coverslip surface through histidine residue tags (H6) at its C-terminus, leaving its cytoplasmic domain free to interact with the recombinant Sx1A (Sx1A-H6) that is similarly attached by means of a C-terminus histidine tag to the nickel-coated cantilever tip. These two proteins are brought to near proximity (approach; *arrow pointing down*) by means of the piezoelectric element and then taken apart (retract; *arrow pointing up*). (*B*) Bright-field images of the cantilevers that were subjected to indirect immunochemistry in *C*. Cantilevers incubated with Sx1A-H6 (+) were successfully functionalized as indicated by the positive immunoreactivity when compared to the control cantilevers where Sx1A-H6 (−) was omitted from the incubation solution (*C*). (*D*) Coverslips functionalized with Sb2-H6 (+) showed positive immunoreactivity when compared to control coverslips where Sb2-H6 (−) was not attached to the coverslip. (*E*) The retraction part of a typical force-distance (extension) curve using a Sx1A-H6 functionalized tip and a Sb2-H6 functionalized coverslip. In the segments *ab* and *bc* (see ''Results'' for details), the coverslip and the cantilever tip are still in contact. The Sx1A-Sb2 intermolecular bond starts to be extended at point *d*, which represents the point of zero separation distance between the tip and coverslip. The increasing extension as the coverslip moves further away from the tip leads to increased application of the force on the intermolecular bond until it ruptures at point *e*. The segment *ef* is then the measure of the force (ordinate) necessary to remove Sx1A-Sb2 interaction. The extension induced can be calculated from the *z*-axis distance moved by the piezo (abscissa) given by segment *de*. In the example shown in *E* the force measures 237 pN, whereas the extension at rupture is 23 nm. The dashed line indicates zero force, whereas its intercept with the force-distance curve indicates point *b*. Circles indicate different points within the force-distance curve. Distributions of the forces and corresponding extensions at rupture for Sx1A-Sb2 single intermolecular bonds are shown in *F* and *G*, respectively. Arrowheads in *F* and *G* indicate the mean values. The drawing in *A* is not to scale. Retraction velocity, 1.6 μm/s. Scale bar, 30 μm in *B* and *C*, whereas 10 μm in *D*.

(Fig. 1). We coated glass coverslips and microfabricated AFM cantilever tips with nickel films, which were partially oxidized by exposure to air (44). The nickel-coated glass coverslips were functionalized with recombinant Sb2 (rat sequence aa 1–94) conjugated to six consecutive histidine molecules (H6) tag at its C-terminus (Sb2-H6) (40); the H6 was sterically coordinated by Ni^{2+} generated from nickel oxidation. To study Sb's interaction with Sx1A we used nickel-coated AFM tips functionalized with a recombinant Sx1A (rat sequence aa 1–266) conjugated to an H6 tag at its C-terminus (Sx1A-H6) (39). Success in coupling of recombinant proteins to their respective surfaces was assessed using indirect immunochemistry. Monoclonal antibody against Sx (49) revealed the presence of Sx1A-H6 recombinant protein only on functionalized cantilevers, but not on the control cantilevers, where recombinant proteins were omitted during the functionalization procedure (Fig. 1, B and C). Similarly, incubation of nickel-coated glass coverslips with recombinant Sb2-H6 resulted in functionalization of glass surface (Fig. 1 D) as detected by a monoclonal antibody directed against Sb2 (42). As both SNARE proteins were tagged at their C-termini, their parts corresponding to cytoplasmic tails were freely available for intermolecular interactions. A standard AFM with a fluid cell containing internal saline was used to measure the strength of the single intermolecular interactions. The functionalized coverslip was mounted on top of the piezoelectric tube, whereas the functionalized AFM cantilever was mounted on the fluid cell. The piezo was then used to move the functionalized coverslip toward and away from the cantilever tip. The interaction force was measured from the deflection of the cantilever. Sx1A and Sb2 were brought in contact by means of the piezo; the contact force was between 0.75 and 1.2 nN, whereas the contact time varied between 0.5 and 3 s depending on the force loading rate. As the coverslip was moved down starting at point a in Fig. 1 E, it remained attached to the tip until point c. The straight line trace ab is due to the linear response of the tip in rigid contact with the coverslip. The segment bc, recorded as an increase in force, represents bending of a cantilever due to nonspecific interactions between the tip and the coverslip. These interactions were recorded at all times even when probing nonfunctionalized nickel-coated glass coverslips with nickel-coated tips (Fig. 2; Table 1). At point c in Fig. 1 E the tip instantaneously snaps away from the coverslip (zero extension) and point d is the start of the observed stretching of the bound proteins due to the continued movement of the coverslip. The (nonzero) extension of the proteins observed after point d is absent in experiments where the bound protein system did not form (determining the interaction probability) or was absent (control experiments; see below and Table 2). In ~38% of attempts, ranging from 32% to 48% for different sets of functionalized tips and coverslips, we detected an interaction force due to bonding between two proteins. The intermolecular bond was stretched at a retraction velocity of 1.6 μm/s, leading to its rupture at a defined force
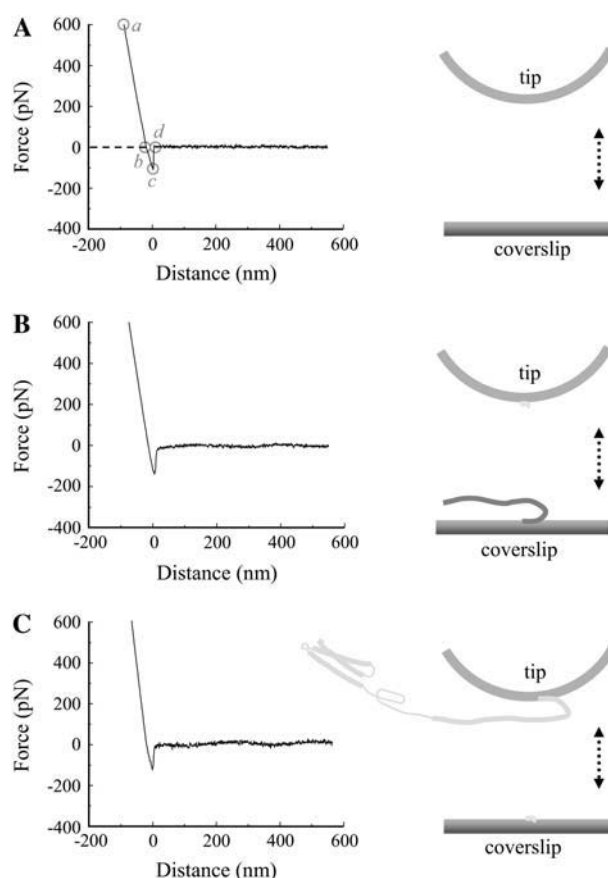

FIGURE 2 Nonspecific interactions between the tips and coverslips. (A) The retraction part of a typical force-distance curve acquired using nickel-coated tips and coverslips. In the segments ab and bc, the coverslip and the cantilever tip are still in contact, until they separate, as indicated by the segment cd with force returning to zero at point d. The dashed line indicates zero force, whereas its intercept with the force-distance curve indicates point b. Circles indicate the different points within the force-distance curve. Similar force-distance curves were recorded when H6 functionalized tips were used to probe Sb2-H6 functionalized coverslips (B) or when Sx1A-H6 functionalized tips were used to probe H6 functionalized coverslips (C; also see Table 1). Drawings are not to scale. Retraction velocity, 1.6 μm/s.

and at a finite distance (extension) from the glass surface (237 ± 4 pN and 23.0 ± 0.6 nm, respectively; 456 events; Fig. 1, E–G). This rupture force and the corresponding mechanical extension of the complex when integrated provide the free energy change for breaking the bonds. Although a considerable fraction of the force is expended to stretching the molecules against the entropic elasticity, the force-distance (extension) relationship (Fig. 1 E, de segment) could not be well explained by the worm-like chain polymer model (50,51), as only the stiff asymptotic section of the polymer extension was present. Therefore, the interacting Sx1A-Sb2 molecular pair does not have any free wriggling polymer sections, implying that these molecules are completely zippered. Although the long mechanical extension of ~23 nm prevents classification of these interactions as arising from narrow angstrom (Å) size potential barriers

TABLE 1 Nonspecific interactions between tips and coverslips

Tip	Coverslip	Positive	Tested	Positive (%)
Ni^{2+}	Ni^{2+}	350	350	100.0
Sx1A-H6	Sb2-H6	465	468	99.4
H6	Sb2-H6	200	200	100.0
Sx1A-H6	H6	320	320	100.0
Sx1A-H6 + GST-Sb2	Sb2-H6	1478	1482	99.7
Sx1A-H6	Sb2-H6 + GST-Sx1A	1372	1378	99.6
Sx1A-H6 + Sb2-H6	Sb2-H6	498	500	99.6
Sx1A-H6	Sb2-H6 + Sx1A-H6	493	494	99.8

Note: Nonspecific interactions refer to the *bcd* segment of the force-distance curves (see Figs. 1 *E* and 2 *A*); retraction velocity is 1.6 μm/s.

Abbreviations: GST, glutathione S-transferase; H6, six consecutive histidines tag; Sb2, synaptobrevin 2; Sx1A, syntaxin 1A.

previously noted in other single molecular bond measurements (34,52,53), it provides insight into the nature of the intermolecular interaction helping to distinguish between a zippering type (formation of coiled coils) and that due to a localized binding site. This extension in Sx1A-Sb2 interactions favors a model where zippering spans the entire SNARE domains of these molecules up to their C-termini. Since Sx1A used here should be in closed form as the construct encompasses entire cytoplasmic tail including regulatory N-terminal domain, the existence of Sx1A-Sb2 interactions indicate that either Sb2 induces a conformational change of Sx1A to bring it to open state or Sb2 can directly interact with the closed form of Sx, as recently suggested ((19,54), also see below).

To verify specificity of the interactions between Sx1A and Sb2, we performed control experiments with tips or coverslips functionalized with H6 (Table 2). Here, we probed Sb2-

TABLE 2 Specific interactions between syntaxin 1A and synaptobrevin 2

Tip	Coverslip	Positive	Tested	Positive (%)
Ni^{2+}	Ni^{2+}	0	350	0
Sx1A-H6	Sb2-H6	2146	5652	38
H6	Sb2-H6	1	200	<1
Sx1A-H6	H6	2	320	<1
Sx1A-H6	Sb2-H6	65	182	36
Sx1A-H6 + GST-Sb2	Sb2-H6	71	1482	5
Sx1A-H6 + GST	Sb2-H6	194	494	39
Sx1A-H6	Sb2-H6	105	286	37
Sx1A-H6	Sb2-H6 + GST-Sx1A	72	1378	5
Sx1A-H6	Sb2-H6 + GST	174	494	35
Sx1A-H6	Sb2-H6	341	1010	34
Sx1A-H6 + Sb2-H6	Sb2-H6	14	500	3
Sx1A-H6	Sb2-H6 + Sx1A-H6	21	494	4

Note: specific interactions refer to the *def* segment of the force-distance curves (see Figs. 1 *E* and 2 *A*); retraction velocity is 1.6 μm/s; spaces separate matching sets of experiments.

Abbreviations: GST, glutathione S-transferase; H6, six consecutive histidines tag; Sb2, synaptobrevin 2; Sx1A, syntaxin 1A.

H6 functionalized coverslips with H6 functionalized tips. Alternatively we used Sx1A-H6 functionalized tips to probe H6 functionalized coverslips. Although we recorded at all times nonspecific interactions described in Figs. 1 and 2 as the segment *bcd* (Table 1), the nonzero extensions (after point *d*, segment *def*) were recorded in <1% of attempts, as compared to 38% in controls where Sx1A-H6 functionalized tips and Sb2-H6 functionalized coverslips were used. Additionally, parallel experiments involving soluble SNARE cytoplasmic tails as competitive antagonists were performed (Table 2). Here, we preincubated Sx1A-H6 functionalized tips with GST-Sb2, and then used these tips to probe Sb2-H6 functionalized coverslips. We also preincubated Sb2-H6 functionalized coverslips with GST-Sx1A, which were then probed with Sx1A-H6 functionalized tips. We find that this treatment of functionalized tips and coverslips with soluble (GST-tagged) complementary SNARE cytoplasmic tails, but not with GST alone, caused great reduction in interactions between Sx1A and Sb2 as compared to control (Table 2). One concern with these experiments is the possibility that GST moiety of chimeric proteins is sterically hindering binding between proteins on the tip and coverslips, whereas complementary cytoplasmic tails serve as the means to deliver it to specific site of interaction. To address this possibility, we cofunctionalized tips with Sx1A-H6 + Sb2-H6, which were then used to probe coverslips functionalized with Sb2-H6, and, conversely, we cofunctionalized coverslips with Sb2-H6 + Sx1A-H6, which were probed with Sx1A-H6 functionalized tips. We find that this treatment of cofunctionalized tips and coverslips with H6-tagged complementary SNARE cytoplasmic tails caused great reduction in interactions between Sx1A and Sb2 as compared to control (Table 2); again, nonspecific interactions were recorded essentially at all times (Table 1). Taken together these data indicate that Sb2-H6 and Sx1A-H6 are selectively immobilized via H6, but not through nonspecific adsorption.

To further study the specificity of the interaction between Sx1A and Sb2, we used the light chain of BoNT-B, which can cleave Sb2 (55–57), and thus can reduce the probability of interactions between Sx1A and Sb2. We first verified that BoNT-B, a Zn^{2+} endopeptidase, in the presence of zinc ions cleaves immobilized Sb2 by using immunochemistry and Western blots (Fig. 3). In parallel, we recorded force-distance curves. After determining a baseline probability of interactions occurring between Sx1A and Sb2 (35%; Table 3), a solution containing BoNT-B (18 nM) and zinc ions (44 μM) was introduced into the fluid cell while measuring intermolecular interactions. The ratio of positive interactions after and before the treatment (Table 3, A/B, 0.2) indicates that the cleavage of the Sb2 led to the large reduction in the number of Sx1A-Sb2 interactions, when compared to the sham treatment where a plain solution was injected (Table 3, sham, A/B, 1.1). Zinc ions alone did not affect the probability of Sx1A-Sb2 intermolecular interactions. Native light chain of BoNT-B, however, caused a small reduction in the number
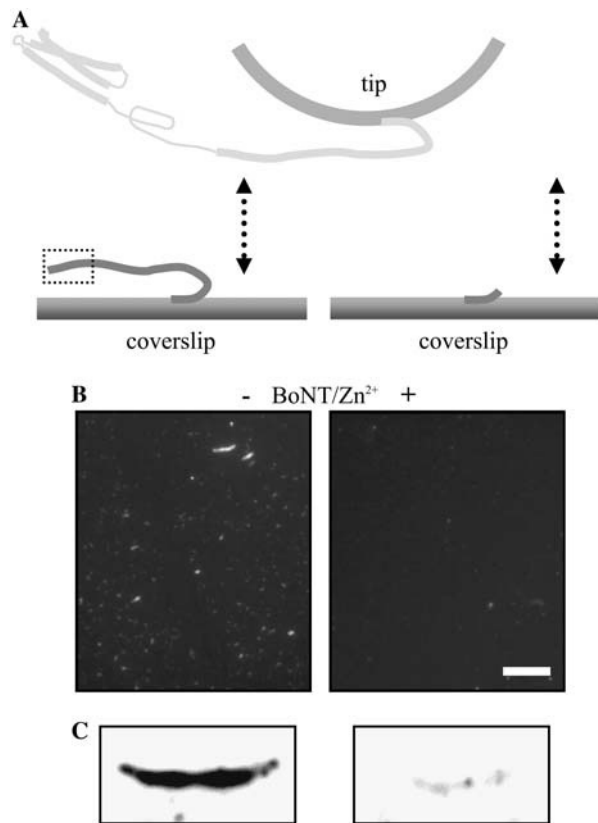
FIGURE 3 Specificity of the extension and force measurements. (*A*) BoNT-B in the presence of zinc ions (Zn^{2+}) cleaves recombinant Sb2 as revealed by the reduction in Sb2 immunoreactivity on functionalized coverslips (*B*, +) and by the reduction of Sb2 immunoreactive band on Western blots (*C*, +) when compared to their controls (*B* and *C*, −). Dashed box in *A* indicates epitope recognized by anti-Sb2 antibody (for details see ''Materials and Methods''). The drawing in *A* is not to scale. Scale bar in *B*, 10 μm.

of interactions (Table 3, A/B, 0.8). This marginal action of native BoNT-B was sensitive to the presence of the Zn^{2+} chelator TPEN (9 μM), which itself did not cause an effect on the probability of Sx1A-Sb2 interactions. Thus, BoNT-B in its native form had some prebound Zn^{2+}, as

TABLE 3 Botulinum neurotoxin type B affects the interaction between syntaxin 1A and synaptobrevin 2

Treatment	Before (B)			After (A)			
	Positive	Total	Positive B (%)	Positive	Total	Positive A (%)	A/B
Sham	80	234	34	75	208	36	1.1
BoNT-B	222	624	36	193	678	28	0.8
BoNT-B + Zn^{2+}	138	390	35	82	1170	7	0.2
Zn^{2+}	84	234	36	85	234	36	1.0
BoNT-B + TPEN	82	234	35	89	260	34	1.0
TPEN	89	234	38	98	260	38	1.0

Note: Sham represents a control for the injection of the reagents (treatment) into the AFM fluid chamber (for details see Materials and Methods).
Abbreviations: BoNT-B, botulinum neurotoxin type B; TPEN, tetrakis-(2-pyridilmethyl)ethylenediamine.

described previously for native light chains of various Clostridial toxins (58–60). Taken together, the sensitivity of Sx1A-Sb2 interactions to BoNT-B confirms the specificity of our measurements.

Additional test of the Sx1A-Sb2 interaction specificity was done. Here the cantilever tips were functionalized using a truncated form of Sx, $Sx1A_{178-266}$-H6, encoding for rat aa 178–266, thus, lacking a part of the molecule N-terminally from its SNARE domain, and used to probe Sb2-H6 functionalized glass coverslips (Fig. 4 *A*). We recorded the interaction forces and extension values in 37% of attempts (239 of 650). These measurements were not significantly different from those acquired using a Sx1A molecule (aa 1–266) containing the entire cytoplasmic domain (compare Fig. 4 *E* with Fig. 1, *F* and *G*; also see Fig. 6 *D*), a finding that is consistent with previous reports indicating necessity of SNARE domain, but not of deleted section of Sx1A molecule (aa 1–177) for Sx1A-Sb2 interactions (30,38,61). Interestingly, both Sx1A and $Sx1A_{178-266}$ interacted with Sb2 with similar probability, as the interactions were recorded in 38% and 37% of attempts, respectively. This favors the notion that Sb2 directly interacts with the SNARE domain of Sx1A in closed form, without inducing a large conformation change of Sx1A from its closed to open state.

After this initial confirmation of the specificity of measured interactions, we further studied the properties of Sx1A-Sb2 interactions. In this set of experiments we incubated Sb2-H6 functionalized coverslips with synthetic peptides encoding for parts of the rat Sx1A sequence, either aa 178–200 or aa 215–235 (Fig. 5 *A*). After preincubation with peptides we probed Sb2-H6 functionalized coverslips with Sx1A-H6 functionalized tips. We found that the peptide aa 215–235 that putatively binds closer to the C-terminus of Sb2 reduces the number of Sx1A-Sb2 interactions more frequently (9% of events recorded) than the peptide aa 178–200 which binds to the N-terminus of Sb2 (30% of events recorded as compared to 43% in control without peptide preincubation; Fig. 5 *B*). Thus, the disruption of the Sx1A-Sb2 interaction was enhanced if the binding of a Sx1A cognate peptide occurred closer to the C-terminus of Sb2, hence, closer to the starting point of the extension. Additionally, we recorded the position-dependent shortening of the Sx1A-Sb2 extension, where, although reduced in number, successful interactions in the presence of aa 215–235 measured 14.6 ± 0.8 nm ($n = 138$), whereas 20.0 ± 0.7 nm ($n = 270$) in the presence of aa 178–200 (compare Fig. 5, *C* and *D*); both extension measurements were significantly shorter than the 23.0 ± 0.6 nm in control measurements without peptide incubation (compare Fig. 1 *F* and Fig. 5 *E*, left; also see Fig. 6 *D*). These data further indicate that Sx1A-Sb2 interaction encompassed the entire length of their SNARE domains, which are zippered without the presence of SNAP25.

After the study of mechanical properties for Sx1A-Sb2 intermolecular interactions, we then measured the single intermolecular interaction events between all three core proteins
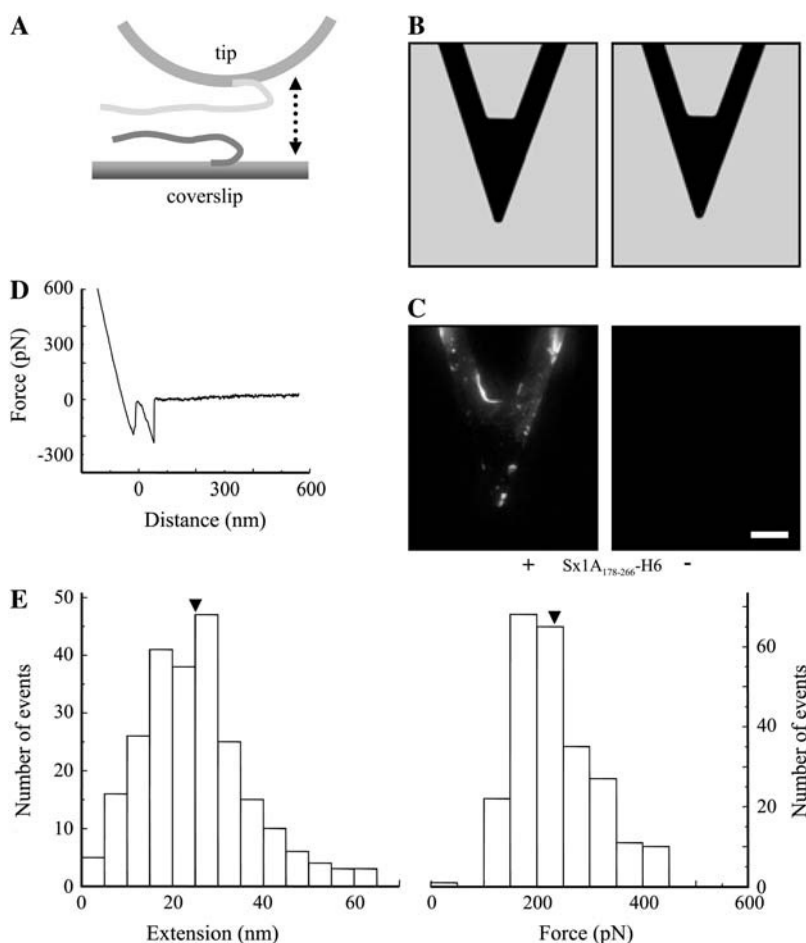
FIGURE 4 The SNARE domain of Sx1A is sufficient for interaction with Sb2. (*A*) Cantilevers incubated with $Sx1A_{178-266}$-H6 (+), a truncated form of Sx1A encoding for rat sequence aa 178–266 and containing SNARE domain, but lacking the remaining N-terminal part of the Sx1A molecule, were successfully functionalized as indicated by the positive immunoreactivity (*C*) when compared to the control cantilevers where $Sx1A_{178-266}$-H6 (−) was not attached to the cantilever. (*B*) Bright-field images of cantilevers that were subjected to indirect immunochemistry in *C*. (*D*) The retraction part of a typical force-distance curve using a truncated $Sx1A_{178-266}$-H6 functionalized tip and a Sb2-H6 functionalized coverslip. (*E*) Distributions of the extensions and forces at rupture recorded from the interactions between $Sx1A_{178-266}$-H6 functionalized tips and Sb2-H6 functionalized coverslips indicate that the SNARE domain of Sx1A is sufficient for interactions with Sb2, whereas the remaining part of Sx1A (aa 1–177) is not necessary for these intermolecular interactions to occur (compare with Fig. 1, *F* and *G*). Arrowheads in *E* indicate mean values. Drawing in *A* is not to scale. Retraction velocity, 1.6 μm/s. Scale bars in *B* and *C*, 30 μm.

of the SNARE complex, Sb2, Sx1A, and SNAP25B. Here, the AFM cantilevers were functionalized with Sx1A-H6 and then preincubated with SNAP25B having GST at its N-terminus (GST-SNAP25B) to form a binary complex, whereas the nickel-coated coverslips were functionalized with Sb2-H6 (Fig. 6 *A*, *top*). We confirmed the formation of the binary complex at the AFM cantilevers using indirect immunochemistry (Fig. 6 *A*, *bottom*). Next, we loaded both a tip and a coverslip into the fluid cell and brought the coverslip into contact with the tip. At the contact site with the plate a binary Sx1A-SNAP25B complex at the tip binds Sb2 on the coverslip to form a ternary Sb2-Sx1A-SNAP25B core SNARE complex. Retracting the coverslip dissociated this complex, while we measured the extension and rupture force for this type of single intermolecular interaction (Fig. 6, *B* and *C*). SNAP25B had little effect on the probability of Sx1A-Sb2 interactions, since we measured them in 40% of attempts (272 of 676), a finding consistent with the lack of effect by SNAP25 on docking efficiency and the probability of thermally induced liposome-bilayer fusion (19). Although the presence of GST-SNAP25B on the tip did not cause any changes in force measurements (243 ± 5 pN, 272 events; Fig. 6, *B–D*) at ~20 nN/s force loading rate (but see below

for different rates), the extension measurements exhibited significant shortening (12.5 ± 0.4 nm, 272 events) when compared to the control Sx1A-Sb2 interactions (23.0 ± 0.6 nm). In contrast, when Sx1A-H6 functionalized tips were preincubated with GST, in 39% of attempts (192 of 494) we observed the force and extension measurements (234 ± 7 pN and 22.8 ± 0.7 nm, 192 events), which were not significantly different from measurements in the control experiments recording Sx1A-Sb2 interactions (Fig. 6, *B* and *C*; also compare Fig. 6 *C*, *middle*, with Fig. 1 *F*). Additionally, we prepared AFM tips functionalized with $Sx1A_{178-266}$-H6 that were preincubated with GST-SNAP25B and used to probe Sb2 functionalized glass coverslips. In 39% of attempts (173 of 442) we observed force and extension values corresponding to those recorded with complete Sx1A-H6 (compare *bottom* and *top* graphs in Fig. 6, *B* and *C*), indicating that the non-SNARE portion (H_{abc} domain and linker region to the SNARE domain) of the Sx1A molecule does not play a role in the assembly of the core SNARE complex.

One concern with the use of GST-tagged SNAP25B is that GST moieties can dimerize (62). Thus, it is possible that the above data is reporting on the interaction between Sx1A, Sb2, and GST-SNAP25B dimers. Since the use of thrombin
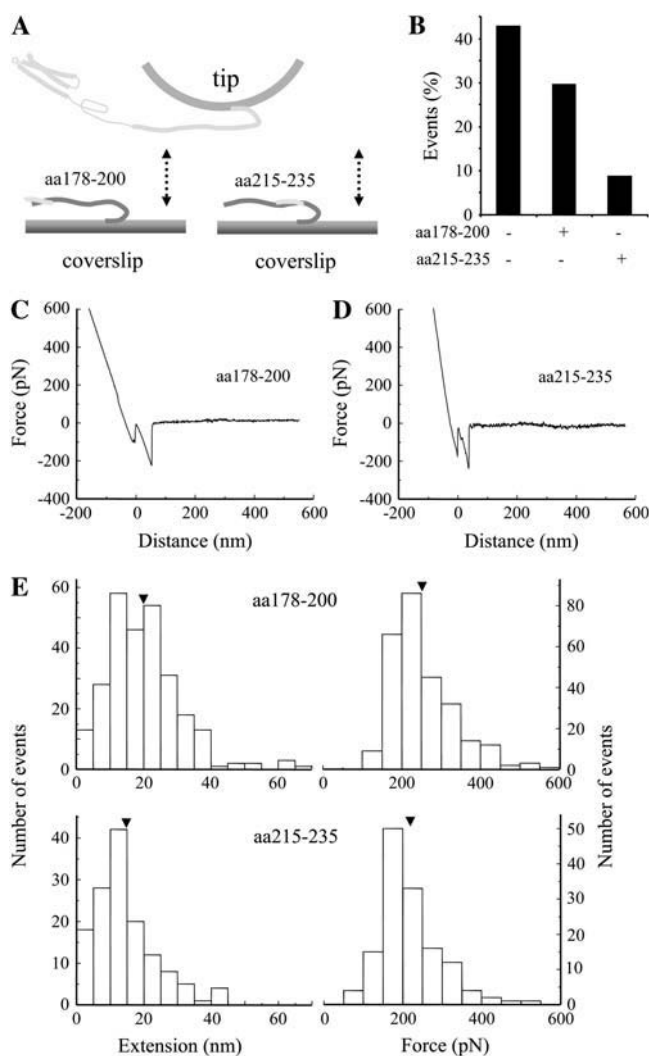
FIGURE 5 Sb2 and Sx1A are zippered. Sb2 functionalized coverslips were preincubated with peptides encoding for a portion of rat Sx1A molecule, either aa 178–200 or aa 215–235 (*A*). Force spectroscopy (*double arrow*) reveals that the number of interactions between Sx1A and Sb2 is reduced in conditions where peptides were preincubated with Sb2 functionalized coverslips (*B*). The retraction part of typical force-distance curves using a Sx1A-H6 functionalized tip and a Sb2-H6 functionalized coverslip preincubated with either aa 178–200 (*C*) or aa 215–235 peptides (*D*). (*E*) Distributions of the extensions and forces at rupture recorded from interactions between Sx1A-Sb2 in the presence of cognate peptides. Arrowheads in *E* indicate mean values. Retraction velocity, 1.6 μm/s. Drawings in *A* are not to scale.

to free SNAP25B from GST-SNAP25B resulted in many proteolytic fragments (data not shown) that may contaminate our measurements, we used H6-SNAP25B to further address the role of SNAP25B in ternary complex (Fig. 7). Here, Sx1A-H6 and H6-SNAP25B were preincubated in equimolar ratio in a tube to form binary complexes, which were then used to cofunctionalize the AFM tips. Coverslips functionalized with Sb2-H6 were probed with cofunctionalized tips.

We found that the presence of H6-SNAP25B on the tip did not cause any changes in the force measurements at ~20 nN/s force loading rate, whereas as before the extension measurements exhibited significant shortening (245 $\pm$ 5 pN, 11.9 $\pm$ 0.4 nm, 206 events; Fig. 7 *E*) when compared to the control where tips were cofunctionalized with Sx1A-H6 and H6 peptide (230 $\pm$ 6 pN, 22.7 $\pm$ 0.6 nm, 120 events; Fig. 7 *E*). Thus, data acquired using H6- and GST-tagged forms of SNAP25B are in full agreement, removing the possibility that in experiments using GST-SNAP25B we were studying the role of its dimer in the ternary complex.

The data we presented in Figs. 1–7 were acquired using a retraction velocity of 1.6 μm/s corresponding to an ~20 nN/s force loading rate. Therefore, to confirm our conclusions with respect to zippering of Sx1A-Sb2 and to further study the nature of interaction within the ternary complex we measured force and extension at the point of rupture of the single intermolecular bond as a function of the force loading rate (Fig. 8). The measured rupture forces increase exponentially with the loading rate (52,53) (one-way ANOVA; $P_{(6,\ 557)} <$ 0.001 and $P_{(7,\ 835)} <$ 0.001 for Sx1A-Sb2 interactions in the absence or presence of GST-SNAP25B, respectively). Extrapolating the force loading rate to zero force enables us to estimate dissociation rates, which correspond to the spontaneous off rates (k_{off}) when only a single barrier width to the transition state exists (63). In the case of Sx1A-Sb2 interaction, this exponential relationship leads to a barrier width of 0.66 Å and a spontaneous dissociation lifetime of 0.16 s based on the assumption of a single barrier (51–53). In contrast the ternary SNARE complex containing Sx1A, Sb2, and SNAP25B is much stronger with a corresponding barrier width of 1.22 Å and a spontaneous lifetime of 2.1 s; hence the ternary SNARE complex is substantially more stable than the Sx1A-Sb2 interaction.

The extension measurements as a function of the force loading rate are even more revealing of the nature of the bonding mechanism in the Sx1A-Sb2 intermolecular bond in comparison to the ternary SNARE complex. The extension in the case of Sx1A-Sb2 exponentially increases as a function of the force loading rate (one-way ANOVA, $P_{(6,\ 557)} <$ 0.001) pointing to the relatively high spontaneous dissociation rate of the zipper-type nonlocalized interaction. In contrast, the extension measurements with the ternary SNARE complex remained constant as the loading rate was varied (one-way ANOVA, $P_{(7,\ 835)} =$ 0.83). The fact that the extension remains constant while the rupture force increases exponentially with the increasing loading rate further points to cuffing, a strong intermolecular binding localized at the 0 layer (also see ''Discussion'') induced by SNAP25B, which concomitantly disturbs the Sx1A-Sb2 prezippered arrangement within their SNARE domains N-terminally to this layer (Fig. 9). Based on the inspection of the force-extension curves, this disturbance of Sx1A-Sb2 interaction N-terminally to the 0 layer caused by SNAP25B is most likely due to unzipping of Sx1A-Sb2, rather than the result of their weak
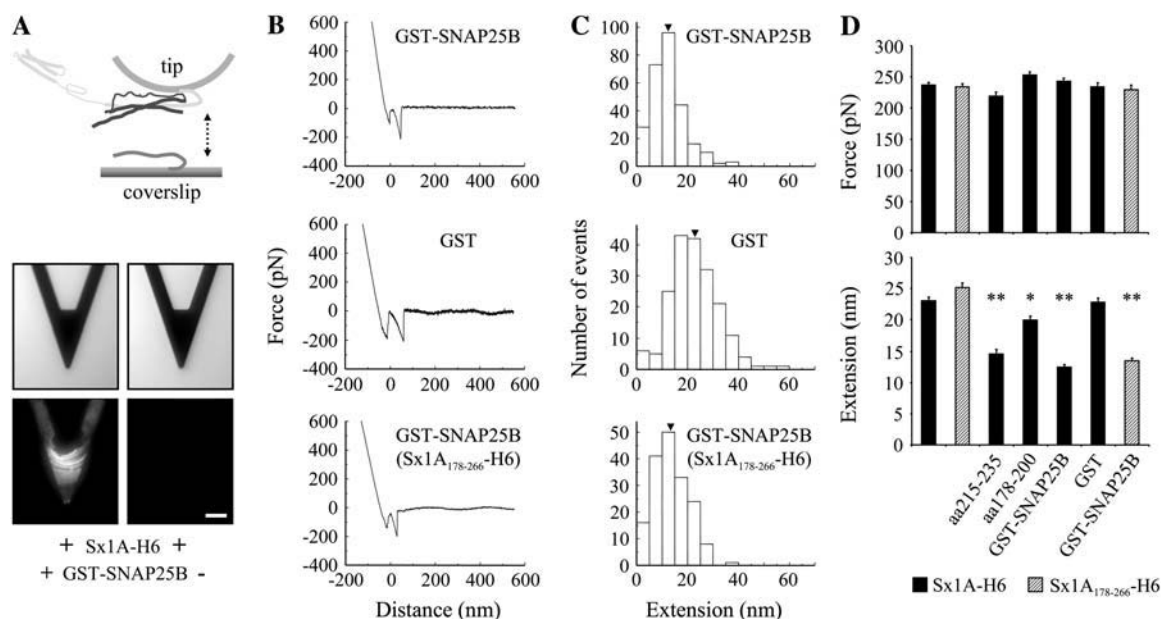
FIGURE 6 SNAP25B reduces the extension of Sx1A-Sb2 interactions. (*A*) Sx1A functionalized tips (Sx1A-H6) were preincubated with GST-SNAP25B. As revealed by indirect immunochemistry (*middle*, bright-field images; *bottom*, fluorescence images) only tips preincubated with GST-SNAP25B (+) show positive immunoreactivity. (*B*) The retraction part of typical force-distance curves and distribution of measured extensions (*C*) when tips were preincubated either with GST-SNAP25B (*top*), GST (*middle*), or where tips were functionalized with truncated $Sx1A_{178-266}$-H6, incubated with GST-SNAP25B, and then used to probe Sb2 functionalized coverslips (*bottom*). (*D*) Summary of all experiments shown in Figs. 1–6 indicate that there is no significant difference in the rupture force in any condition tested (*top*), whereas the extension measurements (*bottom*) are an invaluable tool in the assessment of the functional role of individual SNARE proteins. Arrowheads in *C* indicate mean values. Bars in *D* represent mean ± SE of 138–456 events. Solid bars show data acquired on Sb2-H6 functionalized coverslips probed with Sx1A-H6 functionalized tips, whereas the hatched bars indicate coverslips tested with the truncated form of Sx. Statistical significance was established by a one-way ANOVA followed by a post-hoc Scheffeé's comparison at $P < 0.05$ (*) or $P < 0.01$ (**). Scale bar, 30 μm. Retraction velocity, 1.6 μm/s. Drawing in *A* is not to scale.

interaction, since force-extension curves at different force loads revealed a single unbinding event at ~12 nm without appearance of an additional unbinding event (e.g., at ~23 nm at 20 nN/s).

DISCUSSION

Our data using force spectroscopy are consistent with previous biochemical and x-ray crystallographic findings. However, they also provide additional new insights with regard to the function of these proteins. In previous studies, force spectroscopy was used to study single molecule nanomechanical interactions (33–37), where the rupture force alone was used as the marker of intramolecular and intermolecular mechanical properties. In this study, however, the total extension in addition to the rupture force provides critical information on the binding mechanism between SNARE proteins. Thus, the extension is an important parameter in studying single molecular interaction between proteins, particularly when those proteins are involved in exocytosis, where vesicle-plasma membrane distance is of critical importance.

Interestingly, the force necessary to dismantle a ternary SNARE complex was not significantly larger than the rupture force measured for individual pairs of Sx1A-Sb2 molecules at force loading rate of 20 nN/s (Fig. 6 *D*, *top*, and Fig.

8 *A*; Student's *t*-test, $p > 0.3$). These data are not in complete agreement with a recent report on force measurements of the SNARE complex by others (37). In Fig. 2 of that report, there is an appreciable difference in the rupture force for the various proteins at similar force loading rates (~21 nN/s; calculated from the reported retraction speed of 355 nm/s and spring constant of 0.06 N/m). In our study, however, such force difference is apparent at somewhat lower force loading rates, less than ~7 nN/s (Fig. 8 *A*). For example, at 3 nN/s force loading rate the force to dismantle individual Sx1A-Sb2 pairs was 118 ± 6 pN, whereas the force of 146 ± 6 pN was recorded for disassembling of the ternary complex (Student's *t*-test, $p < 0.01$). Since in both studies the spring constants of the cantilevers were determined using the same method (45), this difference perhaps could be attributed to the method of protein deposition.

Yersin et al. (37) utilized nondirectional cross-linking of the proteins with glutaraldehyde to attach proteins to the surfaces. This procedure tethers proteins to the surface reducing the proteins' ability to mechanically interact, yet it allows them to interact in a random fashion, forming both parallel and antiparallel configurations. In contrast, in our study, we directionally attached proteins with their C-termini containing H6 being sterically coordinated by nickel ions to the surface, thus allowing these proteins to mechanically interact
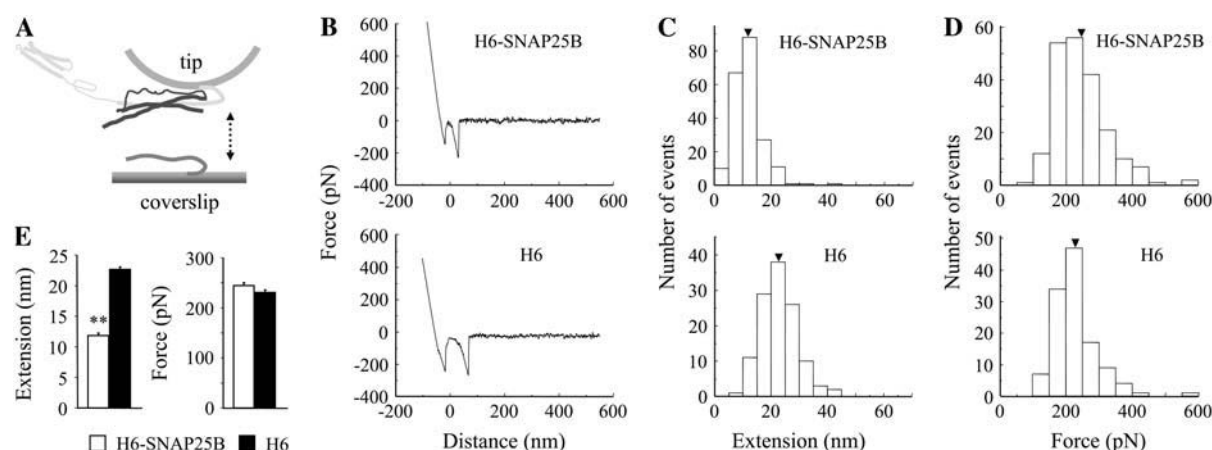
FIGURE 7 H6-SNAP25B reduces the extension of Sx1A-Sb2 interactions. (*A*) Cofunctionalized tips with equimolar ratio of Sx1A-H6/H6-SNAP25B and Sx1A-H6/H6 were used to probe Sb2-H6 functionalized coverslips as shown in the force-distance curves (*B*). Distribution of the measured extensions (*C*) and forces (*D*) at rupture. (*E*) Summary of the experiments indicate that there is no significant difference in the rupture force, whereas there is significant reduction in the extension at rupture when the tips contained Sx1A-H6/H6-SNAP25B, as compared to when the tips were cofunctionalized with Sx1A-H6/H6. Student's *t*-test, $P < 0.01$ (**). Arrowheads in *C* and *D* indicate mean values. Retraction velocity, 1.6 μm/s. Drawing in *A* is not to scale.

in a physiologically more abundant parallel fashion (19,38, 64). Here, as the glass coverslip with deposited Sb2 on its surface is approaching the tip surface covered with Sx1A, the N-termini of these fully extended proteins would start to form parallel interactions at ~20 nm distance between the glass coverslip and the tip, and as this distance shortens, the proteins would become completely zippered. However, for the formation of antiparallel interactions between Sx1A and Sb2, the tip and the glass coverslip would have to be at ~10 nm distance. It is worth noting that these different configurations are a result of interactions between the SNARE domains of Sx1A and Sb2, whereas the N-terminal of SNAP25 remains parallel to Sx1A at all times (32). Since the interconversion between parallel and antiparallel configurations of SNARE complexes had not been observed (32), it is highly likely that we are predominantly recording parallel interactions between the SNARE proteins in all conditions tested. Although we have not directly tested the dominance of the parallel configuration in our study, the experiments carried out elsewhere support this inference. A directed approach using liposome-bilayer fusion showed fivefold numerical preponderance of parallel over antiparallel configuration of SNARE complexes (19), whereas the same proteins exhibited a reverse preponderance where antiparallel configuration was threefold more abundant than parallel when the interactions between proteins where carried out in solution, allowing random interaction (32). Indeed, future carefully designed experiments will need to be performed to determine the contributions of these different states to force and extension measurement using force spectroscopy. Additional benefit of using a directional approach favoring only one configuration of SNARE complex is in its implication of the energy landscape with one stable local minimum and assumption of a single barrier width. Consequently, this permits more accurate assessment of spontaneous dissociation

rates for proteins at a single molecule level than the random approach. More importantly, however, the directed, nickel-histidine coordination approach of protein deposition removes concerns with regard to tethering of proteins to the surface, whereas when a cross-linking technique is used, it inherently reduces protein's ability to mechanically interact, an essential requirement when studying mechanical processes.

As implied above in our experimental approach, we find extension to be the important measurement parameter of the interaction between SNARE complex proteins, as well as the rupture force when experiments were performed over the wide range of different retraction speeds force loading rates. Indeed, the force measurements were also important in a recent BoNT-B micromechanosensor development, since a single molecular pair Sx1A-Sb2 binding force of ~250 pN was sufficient to suspend rather large beads (up to ~41 μM in diameter) on AFM cantilevers, whose timed detachment was a measure of BoNT-B presence (44). Additionally, the force measurements indicate that the strength of interaction between molecules in single Sx1A-Sb2 pairs or ternary complexes could easily allow one pair/complex to effectively keep a vesicle attached to the membrane, a finding that is in agreement with the measurements using FRET approach elsewhere, showing that 1–2 ternary SNARE complex interactions were sufficient for a single liposome docking (19).

The large extension of 23 nm measured in the Sx1A-Sb2 interaction together with the ability to cause its alteration when incubated with Sx1A cognate peptides and its exponential relation to the force loading rate, indicates that the region of this interaction encompasses the entire SNARE domains of these two proteins (Figs. 1, 5, and 8). If we consider that amino acid to amino acid distance within the coil is 0.15 nm, then ~150 aa would be involved in this interaction, perhaps ~75 aa on each protein. This is consistent with previous reports that minimum binding sites between Sx-Sb2
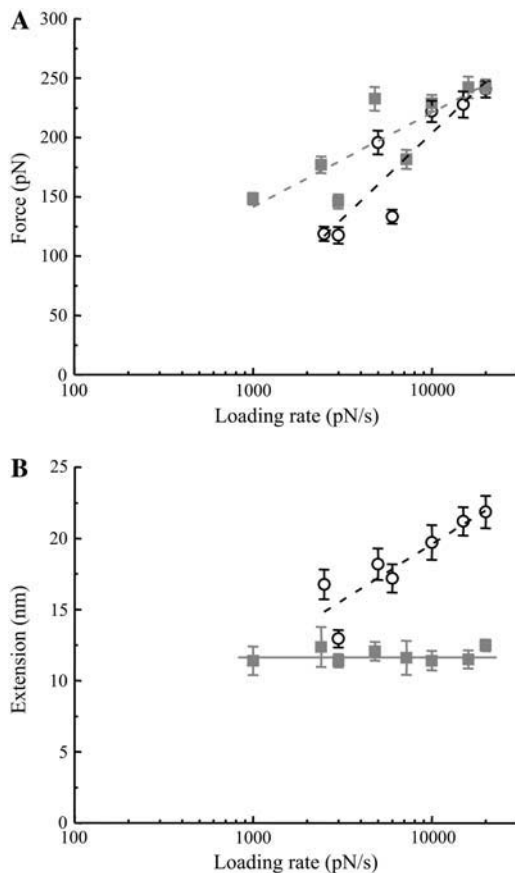
FIGURE 9 A model describing interactions between SNARE proteins. Sx1A and Sb2 are zippered through their entire SNARE domains (*left*). When SNAP25B is additionally present within the complex (*right*), the interaction is localized C-terminally from a Sx1A-Sb2 cuffing position at the 0 layer (*circle*), whereas N-terminally from there Sx1A and Sb2 are either unzippered or very weakly bound (*arrow*), allowing a possible interaction with additional proteins. Drawings are not to scale.

FIGURE 8 The force and extension values for dissociation of SNARE proteins as a function of the force loading rate. (*A*) The force necessary to take apart the Sx1A-Sb2 in the absence (*circles*) or presence of SNAP25B (*squares*) increases exponentially with the increase in the loading rate. (*B*) The extension changes significantly with the loading rate only when Sx1A-Sb2 interactions are ruptured, but not when SNAP25B is present with Sx1A-Sb2. Points represent mean $\pm$ SE (61–100 events in *A* and 33–272 events in *B*). The dashed lines indicate fits to the data described by either an equation force = $a + b \times$ ln (force loading rate) in *A*, where $a = -373$ pN and -96 pN, whereas $b = 63$ pN and 34 pN, for Sx1A-Sb2 ($r = 0.9$), and Sx1A-Sb2-SNAP25 ($r = 0.84$) interactions, respectively, or an equation extension = $a + b \times$ ln (force loading rate) in *B*, where a = -12.0 nm and $b = 3.4$ nm for Sx1A-Sb2 interactions ($r = 0.89$). The force loading rate is in pN/s. The solid line indicates that the extension value is constant at 11.6 nm as it does not change with the loading rate when measuring the Sx1A-Sb2-SNAP25B interactions.

include at least 60–70 aa interactions, Sb2 aa 27–94, and Sx aa 190–266 (38,65). However, some helical segments could be extended due to the stretching process, which could break the intramoleculer hydrogen bonds even before the final rupture of the intermolecular bonds. This might explain the broad distribution in the observed rupture forces and extensions shown in Fig. 1, *F* and *G*. It is unlikely that all the hydrogen bonds of the helix are broken as then the total extension required would be approximately double of that observed.

The extension necessary to rupture the Sx1A-Sb2-SNAP25B bond correlates well with crystallographic struc-
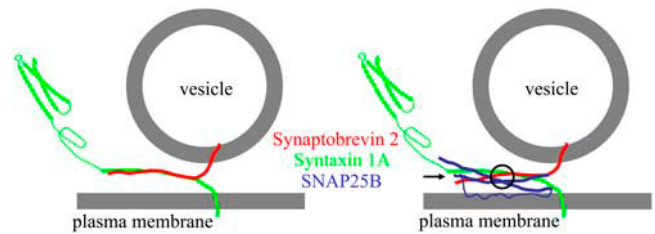
ture of the SNARE complex reported elsewhere (consult Fig. 2 of Sutton et al. (31)). In the SNARE complex, four α helices (Sb2 and Sx each contributing one helix, whereas SNAP25 two) are knitted together by hydrophobic interactions, with an ionic interaction at the 0 layer (Figs. 2 and 3 of Sutton et al. (31)). The flanking leucine zipper layers with hydrophobic interaction act as a water-tight seal to shield the ionic interactions from the surrounding aqueous medium. This seal stabilizes the four helical oligomeric state and the register of the complex by decreasing the local dielectric constant by a factor of 80, thereby enhancing the electrostatic interaction within the ionic layer. On applying force to Sx1A and Sb2 at their C-termini, the hydrophobic bonds starting at layer $+8$ are successively broken until layer 0 comes into contact with water, reducing the electrostatic bond strength and leading to the rupture of the complex. If all eight helical turns from each of Sx, Sb2, and two SNAP25 helices that are hydrophobically bonded and precede the ionic bond at 0 layer are completely ruptured and extended under the applied force in our experimental conditions, then the total extension would be 17.3 nm (4 helices $\times$ 8 turns $\times$ 0.54, where 0.54 nm is the pitch of the α-helix (66,67)). This value is somewhat longer than the mean of the extension (12.5 nm in Fig. 6 and 11.9 nm in Fig. 7) measured in our experiments, and it may indicate that only partial extension of the SNARE complex is necessary to destroy the water-tight seal, leading to rupture of the bond. A second possibility is that the ruptured sections of the molecules are not aligned with the tip-coverslip axis. A third possibility would be that SNAP25 coils do not make a major contribution to extension measurements, but only the Sx1A and Sb2 coils. Hence, if one uses Arg-56 of Sb2 and Gln-226 of Sx1A as the alignment mark of the 0 layer of the SNARE complex, we have 39 aa residues (56–94) from Sb2 and 41 aa residues (226–266) from Sx1A that can possibly contribute to the intermolecular interaction spanning from the C-termini of the cytoplasmic tails (excluding histidine tags) to the 0 layer, then the extension would be 12.0 nm (80 aa $\times$ 0.15 nm, where 0.15 nm is the axial distance between two aa residues in the

α-helix (67)), a value which compares favorably to the 11.9–12.5 nm measured (also see Fig. 8 *B*; it is a 11.6 nm constant when measured over wide range of force loads). Thus the extension measurement is complimentary to the crystallographic data of the SNARE complex, and it indicates that SNAP25B functionally cuffs Sb2 and Sx1A at the 0 layer. This cuffing would effectively guarantee keeping the vesicle on an ~12 nm maximal distance from the plasma membrane, as opposed to ~23 nm maximal distance in the absence of SNAP25B. Additionally, the presence of SNAP25B increases the spontaneous lifetime of the ternary SNARE complex (~2.1 s), when compared to that Sx1A-Sb2 interaction alone (~0.16 s).

Taken together, these findings suggest that intracellularly there could be two modes of vesicular positioning in respect to the plasma membrane even when all the proteins of SNARE complex are in parallel configuration, and if Sx1a-Sb2 interactions alone are possible in vivo. At vesicle-plasma membrane distances smaller than ~12 nm, the ternary SNARE complex would play the major role in vesicular positioning, whereas at distances of 12–23 nm this role could be accomplished by Sx1A-Sb2 pairs. In lieu of the voltage-gated Ca^{2+} channels' close proximity to SNARE complexes in nanodomains (68), the vesicles positioned closer to the plasma membrane in the presence of SNAP25 would fuse synchronously, when the intracellular Ca^{2+} levels increase, unlike those vesicles docked at farther and various distances solely using Sx1A-Sb2 interactions. Since SNAP25 has been shown to directly interact with synaptotagmin 1 (22,69–71), it may additionally serve to recruit this Ca^{2+} sensor to the SNARE complex. The exact role for the weak interaction/unzipping of the Sx1A and Sb2 N-terminally to the 0 layer after the binding of SNAP25B needs to be studied further. This could perhaps allow additional interactions with other molecules involved in triggering vesicular fusion. Although the proposed model with two modes of vesicular positioning to the plasma membrane is an exciting possibility, the physiological relevance of Sx1A-Sb2 complex, except in genetically and biochemically manipulated systems, is not readily apparent, since it has been suggested that Sb2 could only be available to interact with Sx1 and SNAP25 after Ca^{2+} increase to micromolar levels (72). Thus, future designed experiments will need to be performed to determine whether Sb2 and Sx can form binary complexes in living cells.

REFERENCES

1. Parpura, V., E. Scemes, and D. C. Spray. 2004. Mechanisms of glutamate release from astrocytes: gap junction ''hemichannels'', purinergic receptors and exocytotic release. *Neurochem. Int.* 45:259–264.

2. Montana, V., Y. Ni, V. Sunjara, X. Hua, and V. Parpura. 2004. Vesicular glutamate transporter-dependent glutamate release from astrocytes. *J. Neurosci.* 24:2633–2642.

3. Sollner, T., S. W. Whiteheart, M. Brunner, H. Erdjument-Bromage, S. Geromanos, P. Tempst, and J. E. Rothman. 1993. SNAP receptors implicated in vesicle targeting and fusion. *Nature.* 362:318–324.

4. Sudhof, T. C., P. De Camilli, H. Niemann, and R. Jahn. 1993. Membrane fusion machinery: insights from synaptic proteins. *Cell.* 75:1–4.

5. Protopopov, V., B. Govindan, P. Novick, and J. E. Gerst. 1993. Homologs of the synaptobrevin/VAMP family of synaptic vesicle proteins function on the late secretory pathway in S. cerevisiae. *Cell.* 74:855–861.

6. Nonet, M. L., O. Saifee, H. Zhao, J. B. Rand, and L. Wei. 1998. Synaptic transmission deficits in Caenorhabditis elegans synaptobrevin mutants. *J. Neurosci.* 18:70–80.

7. Deitcher, D. L., A. Ueda, B. A. Stewart, R. W. Burgess, Y. Kidokoro, and T. L. Schwarz. 1998. Distinct requirements for evoked and spontaneous release of neurotransmitter are revealed by mutations in the *Drosophila* gene neuronal-synaptobrevin. *J. Neurosci.* 18:2028–2039.

8. Sweeney, S. T., K. Broadie, J. Keane, H. Niemann, and C. J. O'Kane. 1995. Targeted expression of tetanus toxin light chain in *Drosophila* specifically eliminates synaptic transmission and causes behavioral defects. *Neuron.* 14:341–351.

9. Broadie, K., A. Prokop, H. J. Bellen, C. J. O'Kane, K. L. Schulze, and S. T. Sweeney. 1995. Syntaxin and synaptobrevin function downstream of vesicle docking in *Drosophila. Neuron.* 15:663–673.

10. Hunt, J. M., K. Bommert, M. P. Charlton, A. Kistner, E. Habermann, G. J. Augustine, and H. Betz. 1994. A post-docking role for synaptobrevin in synaptic vesicle fusion. *Neuron.* 12:1269–1279.

11. Schoch, S., F. Deak, A. Konigstorfer, M. Mozhayeva, Y. Sara, T. C. Sudhof, and E. T. Kavalali. 2001. SNARE function analyzed in synaptobrevin/VAMP knockout mice. *Science.* 294:1117–1122.

12. O'Connor, V., C. Heuss, W. M. De Bello, T. Dresbach, M. P. Charlton, J. H. Hunt, L. L. Pellegrini, A. Hodel, M. M. Burger, H. Betz, G. J. Augustine, and T. Schafer. 1997. Disruption of syntaxin-mediated protein interactions blocks neurotransmitter secretion. *Proc. Natl. Acad. Sci. USA.* 94:12186–12191.

13. Han, X., C. T. Wang, J. Bai, E. R. Chapman, and M. B. Jackson. 2004. Transmembrane segments of syntaxin line the fusion pore of Ca^{2+}-triggered exocytosis. *Science.* 304:289–292.

14. Han, X., and M. B. Jackson. 2005. Electrostatic interactions between the syntaxin membrane anchor and neurotransmitter passing through the fusion pore. *Biophys. J.* 88:L20–L22.

15. Washbourne, P., P. M. Thompson, M. Carta, E. T. Costa, J. R. Mathews, G. Lopez-Bendito, Z. Molnar, M. W. Becher, C. F. Valenzuela, L. D. Partridge, and M. C. Wilson. 2002. Genetic ablation of the t-SNARE SNAP-25 distinguishes mechanisms of neuro-exocytosis. *Nat. Neurosci.* 5:19–26.

16. Bhattacharya, S., B. A. Stewart, B. A. Niemeyer, R. W. Burgess, B. D. McCabe, G. Lin, G. Boulianne, C. J. O'Kane, and T. L. Schwarz. 2002. Members of the synaptobrevin/vesicle-associated membrane protein (VAMP) family in *Drosophila* are functionally interchangeable in vivo for neurotransmitter release and cell viability. *Proc. Natl. Acad. Sci. USA.* 99:13867–13872.

17. McNally, J. M., D. J. Woodbury, and J. R. Lemos. 2004. Syntaxin 1A drives fusion of large dense-core neurosecretory granules into a planar lipid bilayer. *Cell Biochem. Biophys.* 41:11–24.

18. Woodbury, D. J., and K. Rognlien. 2000. The t-SNARE syntaxin is sufficient for spontaneous fusion of synaptic vesicles to planar membranes. *Cell Biol. Int.* 24:809–818.

19. Bowen, M. E., K. Weninger, A. T. Brunger, and S. Chu. 2004. Single molecule observation of liposome-bilayer fusion thermally induced by soluble *N*-ethyl maleimide sensitive-factor attachment protein receptors (SNAREs). *Biophys. J.* 87:3569–3584.

20. Liu, T., W. C. Tucker, A. Bhalla, E. R. Chapman, and J. C. Weisshaar. 2005. SNARE-driven, 25-millisecond vesicle fusion in vitro. *Biophys. J.* 89:2458–2472.

21. Schuette, C. G., K. Hatsuzawa, M. Margittai, A. Stein, D. Riedel, P. Kuster, M. Konig, C. Seidel, and R. Jahn. 2004. Determinants of liposome fusion mediated by synaptic SNARE proteins. *Proc. Natl. Acad. Sci. USA.* 101:2858–2863.

22. Tucker, W. C., T. Weber, and E. R. Chapman. 2004. Reconstitution of Ca^{2+}-regulated membrane fusion by synaptotagmin and SNAREs. *Science.* 304:435–438.

23. Heuser, J. E., and T. S. Reese. 1973. Evidence for recycling of synaptic vesicle membrane during transmitter release at the frog neuromuscular junction. *J. Cell Biol.* 57:315–344.

24. Bruns, D., and R. Jahn. 1995. Real-time measurement of transmitter release from single synaptic vesicles. *Nature.* 377:62–65.

25. Zenisek, D., J. A. Steyer, and W. Almers. 2000. Transport, capture and exocytosis of single synaptic vesicles at active zones. *Nature.* 406:849–854.

26. Klyachko, V. A., and M. B. Jackson. 2002. Capacitance steps and fusion pores of small and large-dense-core vesicles in nerve terminals. *Nature.* 418:89–92.

27. Ryan, T. A., and H. Reuter. 2001. Measurements of vesicle recycling in central neurons. *News Physiol. Sci.* 16:10–14.

28. Hess, S. D., P. A. Doroshenko, and G. J. Augustine. 1993. A functional role for GTP-binding proteins in synaptic vesicle cycling. *Science.* 259:1169–1172.

29. Xia, Z., Q. Zhou, J. Lin, and Y. Liu. 2001. Stable SNARE complex prior to evoked synaptic vesicle fusion revealed by fluorescence resonance energy transfer. *J. Biol. Chem.* 276:1766–1771.

30. Calakos, N., M. K. Bennett, K. E. Peterson, and R. H. Scheller. 1994. Protein-protein interactions contributing to the specificity of intracellular vesicular trafficking. *Science.* 263:1146–1149.

31. Sutton, R. B., D. Fasshauer, R. Jahn, and A. T. Brunger. 1998. Crystal structure of a SNARE complex involved in synaptic exocytosis at 2.4 A resolution. *Nature.* 395:347–353.

32. Weninger, K., M. E. Bowen, S. Chu, and A. T. Brunger. 2003. Single-molecule studies of SNARE complex assembly reveal parallel and antiparallel configurations. *Proc. Natl. Acad. Sci. USA.* 100:14800–14805.

33. Florin, E. L., V. T. Moy, and H. E. Gaub. 1994. Adhesion forces between individual ligand-receptor pairs. *Science.* 264:415–417.

34. Merkel, R. 2001. Force spectroscopy on single passive biomolecules and single biomolecular bonds. *Phys. Rep.* 346:343–385.

35. Lee, G. U., L. A. Chrisey, and R. J. Colton. 1994. Direct measurement of the forces between complementary strands of DNA. *Science.* 266:771–773.

36. Oberhauser, A. F., P. K. Hansma, M. Carrion-Vazquez, and J. M. Fernandez. 2001. Stepwise unfolding of titin under force-clamp atomic force microscopy. *Proc. Natl. Acad. Sci. USA.* 98:468–472.

37. Yersin, A., H. Hirling, P. Steiner, S. Magnin, R. Regazzi, B. Huni, P. Huguenot, P. De los Rios, G. Dietler, S. Catsicas, and S. Kasas. 2003. Interactions between synaptic vesicle fusion proteins explored by atomic force microscopy. *Proc. Natl. Acad. Sci. USA.* 100:8736–8741.

38. Lin, R. C., and R. H. Scheller. 1997. Structural organization of the synaptic exocytosis core complex. *Neuron.* 19:1087–1094.

39. Fasshauer, D., W. Antonin, M. Margittai, S. Pabst, and R. Jahn. 1999. Mixed and non-cognate SNARE complexes. Characterization of assembly and biophysical properties. *J. Biol. Chem.* 274:15440–15446.

40. Margittai, M., H. Otto, and R. Jahn. 1999. A stable interaction between syntaxin 1a and synaptobrevin 2 mediated by their transmembrane domains. *FEBS Lett.* 446:40–44.

41. Schoenle, E. J., L. D. Adams, and D. W. Sammons. 1984. Insulin-induced rapid decrease of a major protein in fat cell plasma membranes. *J. Biol. Chem.* 259:12112–12116.

42. Edelmann, L., P. I. Hanson, E. R. Chapman, and R. Jahn. 1995. Synaptobrevin binding to synaptophysin: a potential mechanism for controlling the exocytotic fusion machine. *EMBO J.* 14:224–231.

43. Parpura, V., Y. Fang, T. Basarsky, R. Jahn, and P. G. Haydon. 1995. Expression of synaptobrevin II, cellubrevin and syntaxin but not SNAP-25 in cultured astrocytes. *FEBS Lett.* 377:489–492.

44. Liu, W., V. Montana, E. R. Chapman, U. Mohideen, and V. Parpura. 2003. Botulinum toxin type B micromechanosensor. *Proc. Natl. Acad. Sci. USA.* 100:13621–13625.

45. Hutter, J. L., and J. Bechhoefer. 1993. Calibration of atomic-force microscope tips. *Rev. Sci. Instrum.* 64:1868–1873.

46. Harris, B. W., F. Chen, and U. Mohideen. 2000. Precision measurement of the Casimir force using gold surfaces. *Phys. Rev. A.* 62:052109.

47. Chen, F., and U. Mohideen. 2001. Fiber optic interferometry for precision measurement of the voltage and frequency dependence of the displacement of piezoelectric tubes. *Rev. Sci. Instrum.* 72:3100–3102.

48. Conti, M., G. Falini, and B. Samori. 2000. How strong is the coordination bond between a histidine tag and Ni-nitrilotriacetate? An experiment of mechanochemistry on single molecules. *Angew. Chem. Int. Ed. Engl.* 39:215–218.

49. Barnstable, C. J., R. Hofstein, and K. Akagawa. 1985. A marker of early amacrine cell development in rat retina. *Brain Res.* 352:286–290.

50. Bustamante, C., J. F. Marko, E. D. Siggia, and S. Smith. 1994. Entropic elasticity of lambda-phage DNA. *Science.* 265:1599–1600.

51. Evans, E., and K. Ritchie. 1999. Strength of a weak bond connecting flexible polymer chains. *Biophys. J.* 76:2439–2447.

52. Evans, E., and K. Ritchie. 1997. Dynamic strength of molecular adhesion bonds. *Biophys. J.* 72:1541–1555.

53. Evans, E. 2001. Probing the relation between force–lifetime–and chemistry in single molecular bonds. *Annu. Rev. Biophys. Biomol. Struct.* 30:105–128.

54. Munson, M., X. Chen, A. E. Cocina, S. M. Schultz, and F. M. Hughson. 2000. Interactions within the yeast t-SNARE Sso1p that control SNARE complex assembly. *Nat. Struct. Biol.* 7:894–902.

55. Schiavo, G., O. Rossetto, F. Benfenati, B. Poulain, and C. Montecucco. 1994. Tetanus and botulinum neurotoxins are zinc proteases specific for components of the neuroexocytosis apparatus. *Ann. N. Y. Acad. Sci.* 710:65–75.

56. Schiavo, G., F. Benfenati, B. Poulain, O. Rossetto, P. Polverino de Laureto, B. R. DasGupta, and C. Montecucco. 1992. Tetanus and botulinum-B neurotoxins block neurotransmitter release by proteolytic cleavage of synaptobrevin. *Nature.* 359:832–835.

57. Jahn, R., and H. Niemann. 1994. Molecular mechanisms of clostridial neurotoxins. *Ann. N. Y. Acad. Sci.* 733:245–255.

58. Schiavo, G., C. C. Shone, O. Rossetto, F. C. Alexander, and C. Montecucco. 1993. Botulinum neurotoxin serotype F is a zinc endo-peptidase specific for VAMP/synaptobrevin. *J. Biol. Chem.* 268: 11516–11519.

59. Schiavo, G., O. Rossetto, A. Santucci, B. R. DasGupta, and C. Montecucco. 1992. Botulinum neurotoxins are zinc proteins. *J. Biol. Chem.* 267:23479–23483.

60. Schiavo, G., B. Poulain, O. Rossetto, F. Benfenati, L. Tauc, and C. Montecucco. 1992. Tetanus toxin is a zinc protein and its inhibition of neurotransmitter release and protease activity depend on zinc. *EMBO J.* 11:3577–3583.

61. Davis, A. F., J. Bai, D. Fasshauer, M. J. Wolowick, J. L. Lewis, and E. R. Chapman. 1999. Kinetics of synaptotagmin responses to Ca^{2+} and assembly with the core SNARE complex onto membranes. *Neuron.* 24:363–376.

62. Vargo, M. A., L. Nguyen, and R. F. Colman. 2004. Subunit interface residues of glutathione S-transferase A1–1 that are important in the monomer-dimer equilibrium. *Biochemistry.* 43:3327–3335.

63. Schwesinger, F., R. Ros, T. Strunz, D. Anselmetti, H. J. Guntherodt, A. Honegger, L. Jermutus, L. Tiefenauer, and A. Pluckthun. 2000. Unbinding forces of single antibody-antigen complexes correlate with their thermal dissociation rates. *Proc. Natl. Acad. Sci. USA.* 97:9972–9977.

64. Hanson, P. I., R. Roth, H. Morisaki, R. Jahn, and J. E. Heuser. 1997. Structure and conformational changes in NSF and its membrane receptor complexes visualized by quick-freeze/deep-etch electron microscopy. *Cell.* 90:523–535.

65. Hayashi, T., H. McMahon, S. Yamasaki, T. Binz, Y. Hata, T. C. Sudhof, and H. Niemann. 1994. Synaptic vesicle membrane fusion complex: action of clostridial neurotoxins on assembly. *EMBO J.* 13:5051–5061.

66. Onoa, B., S. Dumont, J. Liphardt, S. B. Smith, I. Tinoco Jr., and C. Bustamante. 2003. Identifying kinetic barriers to mechanical unfolding of the T. thermophila ribozyme. *Science.* 299:1892–1895.

67. Stryer, L. 1995. Biochemistry. W.H. Freeman, New York.

68. Augustine, G. J. 2001. How does calcium trigger neurotransmitter release? *Curr. Opin. Neurobiol.* 11:320–326.

69. Schiavo, G., G. Stenbeck, J. E. Rothman, and T. H. Sollner. 1997. Binding of the synaptic vesicle v-SNARE, synaptotagmin, to the plasma membrane t-SNARE, SNAP-25, can explain docked vesicles at neurotoxin-treated synapses. *Proc. Natl. Acad. Sci. USA.* 94:997–1001.

70. Chieregatti, E., J. W. Witkin, and G. Baldini. 2002. SNAP-25 and synaptotagmin 1 function in Ca^{2+}-dependent reversible docking of granules to the plasma membrane. *Traffic.* 3:496–511.

71. Bai, J., C. T. Wang, D. A. Richards, M. B. Jackson, and E. R. Chapman. 2004. Fusion pore dynamics are regulated by synaptotagmin*t-SNARE interactions. *Neuron.* 41:929–942.

72. Hu, K., J. Carroll, S. Fedorovich, C. Rickman, A. Sukhodub, and B. Davletov. 2002. Vesicular restriction of synaptobrevin suggests a role for calcium in membrane fusion. *Nature.* 415:646–650.